

Nearest-Neighbor Inter-Intra Contrastive Learning from Unlabeled Videos

David Fan Deyu Yang Xinyu Li Vimal Bhat Rohith MV
Amazon Prime Video

{fandavi, deyu, xxnl, vimalb, kurohith}@amazon.com

Abstract

Contrastive learning has recently narrowed the gap between self-supervised and supervised methods in image and video domain. State-of-the-art video contrastive learning methods such as CVRL and ρ -MoCo spatiotemporally augment two clips from the same video as positives. By only sampling positive clips locally from a single video, these methods neglect other semantically related videos that can also be useful. To address this limitation, we leverage nearest-neighbor videos from the global space as additional positive pairs, thus improving positive key diversity and introducing a more relaxed notion of similarity that extends beyond video and even class boundaries. Our method, Inter-Intra Video Contrastive Learning (IIVCL), improves performance on a range of video tasks.

1. Introduction

The success of supervised deep learning for computer vision can largely be attributed to the availability of large-scale labeled datasets [70, 14, 35, 9, 31], which are difficult and expensive to create. However, progress in compute and model representation capabilities has outpaced progress in dataset creation [57, 9]. Self-supervised learning is the paradigm of learning from *unlabeled* data to decouple reliance upon large-scale labeled datasets. It has already shown great potential in NLP [15, 3] for producing representations that generalize well to multiple tasks.

Recently, a flavor of self-supervised learning known as contrastive learning / instance discrimination [49] has become dominant in vision through works such as MoCo [29, 10] and SimCLR [7, 8] which are competitive with supervised learning in image domain. More recently, contrastive learning works for video such as CVRL [52] and ρ -MoCo [20] are competitive with supervised learning. These works learn a representation from unlabeled data by pulling positive pairs closer and pushing negative samples apart in the embedding space. In the case of video, these positive pairs are generated through random augmentations of sub-clips from the *same* video [52, 20], while clips from other

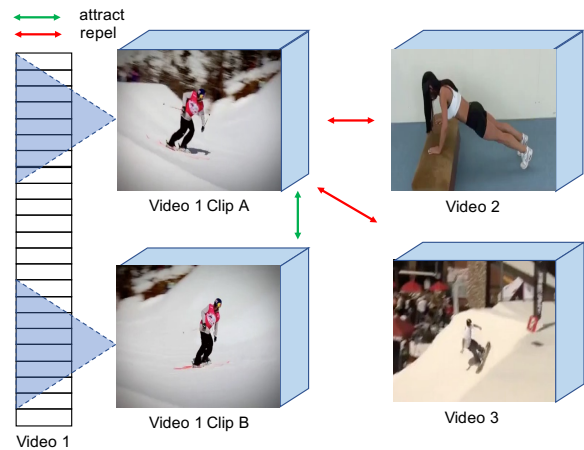


Figure 1: Video contrastive learning methods such as CVRL [52] and ρ -MoCo [20] only sample positive pairs within the same video boundary, such as clips A and B. However, this means that different yet similar videos such as 3 are **never** used as positives, even if they are semantically similar to video 1. Our work leverages semantically similar inter-video pairs as positives (e.g. video 3), in addition to intra-video subclips (e.g. 1.A and 1.B) used by previous works. “Clip” refers to a subset of video frames.

similar videos are *never* used as positives.

By only considering clips that belong to the same video to be positive, works such as CVRL [52] and ρ -MoCo [20] neglect other semantically related videos that may also be useful and relevant as positives for contrastive learning. Fig. 1 depicts such a scenario. Clips A and B from the same skiing video are the positive pair while video 2 (push-up) and video 3 (snowboarding) are negatives. Clips A and B are certainly more similar to each other than to the push-up and snowboarding videos, but the snowboarding video is far more similar to the positive anchor when compared to an indoor activity such as doing push-ups. Yet the relative similarity between skiing - snowboarding will never be exploited by methods such as CVRL [52] and ρ -MoCo [20].

This raises the question of what constitutes a desirable video representation; by focusing too much on local intra-video semantics, we may miss the larger picture and hierarchy of visual concepts. This might lead to overfitting to

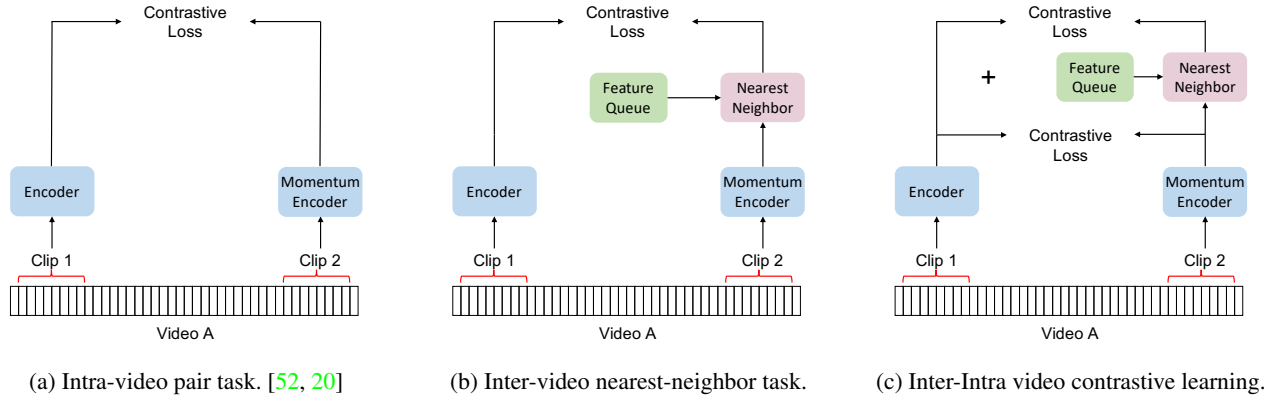


Figure 2: IIVCL Overview. Fig. 2a shows intra-video positive sampling as used by current state-of-the-art [52, 20]. Fig. 2b shows our proposal to leverage nearest-neighbor samples from an evolving queue as positives for contrastive learning. Fig. 2c is our IIVCL which combines a) and b) to learn similarity both within the same video and between different videos. NN sampling is simple, light-weight, and directly plugs into contrastive frameworks. Note that there is no temporal ordering between clips 1 and 2 as they are randomly sampled.

tasks that are similar to the pretraining dataset and thus hurt generalization. On the other hand, if we focus too much on global inter-video semantics, we may lose sight of granular details that are also important for video understanding.

To balance the two, we propose learning notions of similarity both within the same video and between different videos, by leveraging inter-video nearest-neighbor (NNs) from the global space in addition to existing intra-video clips as positive pairs for contrastive learning. For any pair of intra-video clips, our method “Inter-Intra Video Contrastive Learning” (IIVCL) defines a second positive key as the most similar video found from a dynamically evolving queue of randomly sampled videos in the learned representation space, as shown in Fig. 2.

The benefit of adding globally sampled NNs as positives is two-fold. First, NNs present additional diversity in viewpoint and scene orientation, which cannot be expressed through sampling subclips from the *same* video, as shown by comparing Fig. 3 a) and b). This is true whether the subclips are augmented, shuffled or otherwise modified per the pretext task, so long as they belong to the same video. Image works such as NNCLR [18] show that improving positive key diversity leads to better generalization on image tasks, and we explore whether the same is true for video.

Second, because the set of positive keys is expanded beyond the boundaries of a single video, it becomes possible to also learn from weaker yet relevant and useful positive pairs, such as the snowboarding-skiing example from Fig. 1. By combining these nearest-neighbor pairs with intra-video pairs as positives for contrastive learning, the model can learn notions of similarity both within the same video and between different videos, thus striking a balance between learning granular details and learning higher-level visual concepts. We then evaluate whether this leads to im-

proved representations on downstream video tasks.

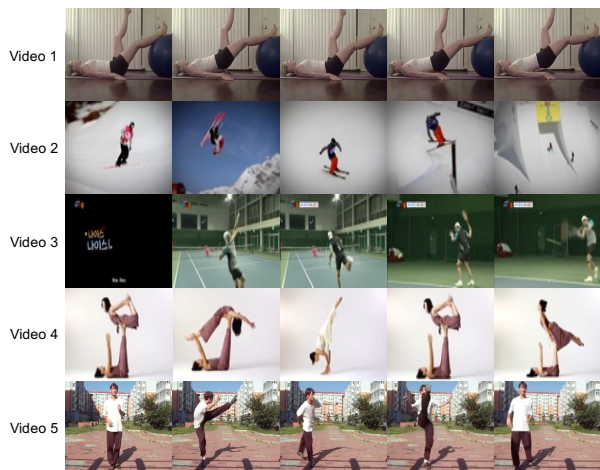
In summary, our contributions are the following:

- (i) Unlike other video-based works, we go beyond single-video positives using only RGB by leveraging globally sampled nearest-neighboring videos as a simple and effective way to increase the semantic diversity of positive keys and introduce higher-level notions of similarity.
- (ii) We introduce IIVCL as a novel yet *simple* self-supervised video representation learning method that learns a joint representation of both intra-video pairs and nearest-neighbors — without clustering nor multiple modalities.
- (iii) We demonstrate that striking a balance between local and global similarity leads to improved performance over existing intra-video contrastive learning methods [52, 20] on video action recognition, action detection, and video retrieval — even in a few-shot learning setting.

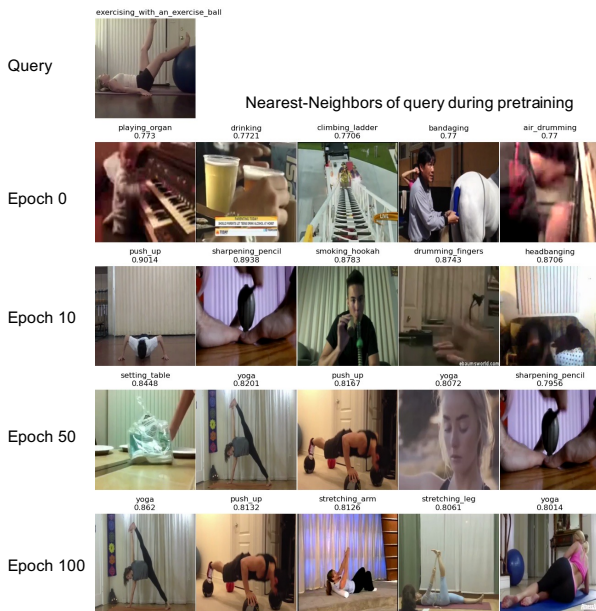
2. Related Work

Self-supervised image representation learning. Earlier works focused on designing pretext tasks whose solution would yield a useful representation for downstream classification. Some pretext tasks include predicting the relative positioning of patches [17], image rotation [22], image colorization [69], solving jigsaw puzzles [47], and counting visual primitives [48]. While promising, these approaches were not competitive with fully-supervised representations [37, 46], partly because it is easy to learn shortcuts that trivially solve the pretext task.

The re-emergence of contrastive learning elevated self-supervised image representation learning as a viable alternative paradigm to fully-supervised learning [29, 10, 7, 8, 24, 11]. These methods encourage models to be invariant to multiple augmented views of the same image. [58] generates multiple views from the same image by splitting im-



(a) Intra-video sampling results in low diversity of positive keys because subclips belong to the same short video. Each row shows a different video.



(b) For a query image (first row), the evolution of the top-5 nearest-neighbors during SSL pretraining starting from random initialization.

Figure 3: Intra-video vs. inter-video nearest-neighbor positives. In a), positive keys are always restricted to a single video boundary, which limits diversity. In b), positive keys are sampled globally using similarity in the learned feature space, which improves during pretraining. NNs do not necessarily belong to the same semantic class as the query. This global notion of similarity improves generalization.

ages into luminance and chrominance space.

Some recent works such as [71, 4, 41] go beyond single-instance contrastive learning by using clusters to find semantically relevant positive pairs. Our work is similar to NNCLR [18] which uses nearest-neighbors for image contrastive learning, but differs in that we combine inter-video nearest-neighbors with intra-video positives for **video** contrastive learning, which brings unique challenges.

Self-supervised video representation learning. Temporal information in videos enables the design of interesting pretext tasks that are not possible with images. Video in general is more challenging due to its temporal dimension. Pretext tasks for video self-supervised learning include predicting future frames [16, 43, 59, 55], the correct order of shuffled frames [44, 21] or shuffled clips [40], video rotation [34], playback speed [2], directionality of video [64], motion and appearance statistics [60], and solving space time cubic puzzles [36]. Other works have leveraged video correspondence by tracking patches [62], pixels [63], and objects [32] across adjacent frames.

Several recent works have considered contrastive learning for video. These methods differ in their definition of positive and negative samples. Some works use different subclips of equal-length from the same video as positive samples [52, 20, 13], or different frames from the same video [58]. [53] samples two subclips of different length

from the same video to encourage generalization to broader context. Other works utilize optical flow in a cross-modal context; [28] uses optical flow to mine RGB images with similar motion cues as positives, while other works do not mine positives but instead learn from the natural correspondence between optical flow and RGB within the same video [65], or within the same frame [58]. Another set of works utilize pretext tasks such as pace prediction [68, 61], clip shuffling [67], or a combination of both [38].

In contrast, our work goes beyond local definitions of positives from a single-video and expands to globally sampled nearest-neighbor videos, but without using optical flow nor separate training phases like [28]. Unlike works such as [5], our work uses the online representation space to pick NNs on the fly instead of pre-computing video clusters. Unlike methods such as [5, 45] that go beyond single-video positives, our work only uses RGB frames.

3. Inter-Intra Video Contrastive Learning

3.1. Contrastive loss

Contrastive learning maximizes the similarity of a given embedded sample q with its embedded positive key k^+ , while minimizing similarity to negative embeddings n_i . In the rest of this work, we refer to (q, k^+) as “positive pairs”. We utilize the InfoNCE loss [49] for self-supervised video

representation learning, which is given below:

$$\mathcal{L}^{\text{NCE}}(q, k^+, \mathcal{N}^-) = -\log \frac{\exp(\text{sim}(q, k^+)/\tau)}{\sum_{k \in \{k^+\} \cup \mathcal{N}^-} \exp(\text{sim}(q, k)/\tau)} \quad (1)$$

where $\tau > 0$ is a temperature hyper-parameter and $\text{sim}(\cdot)$ denotes the similarity function — which in this work is the dot product (cosine) similarity between two ℓ_2 normalized vectors: $\text{sim}(q, k) = q \cdot k = q^T k / (\|q\| \|k\|)$.

3.2. Multi-Task Objective

The manner in which positive pairs are sampled during contrastive learning introduces an inductive bias that has a significant impact on downstream task performance [66]. For example, works such as MoCo [29, 10] and SimCLR [7, 8] that use image augmentation encourage model invariance to different colors, crops, and orientations, potentially at the expense of other inductive bias.

Intra-Video Contrastive Learning. Contrastive learning methods for video such as CVRL [52] and ρ -MoCo [20] use the embeddings of two subclips z_1 and z_2 from the same video as positives. Intra-video positive sampling teaches the model to identify whether two different clips correspond to the same video. Given a queue Q of randomly sampled embeddings, the intra-video contrastive loss is then:

$$\mathcal{L}_{\text{Intra}}(z_1, z_2, Q) = \mathcal{L}^{\text{NCE}}(z_1, z_2, Q) \quad (2)$$

Nearest-Neighbor Contrastive Learning. Motivated by the observation in Fig. 1 that intra-video sampling excludes other semantically similar videos from ever being used as positives; we seek to expand the positive keyset beyond individual video boundaries to improve diversity. Offline positive sets are not suitable because they cannot be efficiently updated at every iteration or even at every epoch. Clustering to find similar videos requires additional hyperparameters. Thus, we maintain a queue Q that is updated with embeddings from each forward pass (design details in Sec. 3.3), which allows us to directly compute cosine similarities between the input video and queue. Given an embedded input video x and queue Q of randomly sampled embeddings across the dataset, we use the nearest-neighbor of x as its positive key:

$$\text{NN}(x, Q) = \underset{z \in Q}{\text{argmax}}(x \cdot z) \quad (3)$$

Let z_1 and z_2 be the embeddings of two subclips from the same video. We use Q for both selecting the NN as a positive key and providing negatives (excluding the NN). Using the nearest-neighbor operation in Eq. 3 to select the positive key for z_1 as $\text{NN}(z_2, Q)$, and removing it from Q to form $Q^- = Q \setminus \text{NN}(z_2, Q)$, we have the NN contrastive loss:

$$\mathcal{L}_{\text{NN}}(z_1, z_2, Q) = \mathcal{L}^{\text{NCE}}(z_1, \text{NN}(z_2, Q), Q^-) \quad (4)$$

Combined Intra and Inter Training Objective

We use the same backbone but separate MLP projection heads to process the intra-video and NN positive pairs. As each of these pretext tasks learns a different notion of similarity, we combine them via a multi-task loss. We also maintain two separate queues of embeddings: Q_{Intra} and Q_{NN} . Q_{NN} is used both to find the NN and provide negative keys (excluding the NN), while Q_{Intra} only provides negative keys. We expand on these details in section 3.3.

Specifically, let $f^q(\cdot)$ and $f^k(\cdot)$ be the encoder and its offline momentum-updated version, $g^{\text{Intra}}(\cdot)$ and $g^{\text{NN}}(\cdot)$ be two separate MLP heads, and x_1 and x_2 be two subclips sampled from the same video. We first obtain the embeddings $(z_1^{\text{Intra}}, z_2^{\text{Intra}})$ and $(z_1^{\text{NN}}, z_2^{\text{NN}})$.

$$\begin{aligned} z_1^{\text{Intra}} &= g^{\text{Intra}}(f^q(x_1)); & z_2^{\text{Intra}} &= g^{\text{Intra}}(f^k(x_2)) \\ z_1^{\text{NN}} &= g^{\text{NN}}(f^q(x_1)); & z_2^{\text{NN}} &= g^{\text{NN}}(f^k(x_2)) \end{aligned}$$

After obtaining the embeddings, we combine Eqs. 2 and 4 to get the final training objective. Note that we use a symmetric loss but show only one side for simplicity. λ_{Intra} and λ_{NN} are tunable parameters that control the contribution of each loss, which in our work is 1.0 for both. An ablation for this is in Tab. 6.

$$\begin{aligned} \mathcal{L}(z_1^{\text{Intra}}, z_2^{\text{Intra}}, z_1^{\text{NN}}, z_2^{\text{NN}}) &= \lambda_{\text{Intra}} \cdot \mathcal{L}_{\text{Intra}}(z_1^{\text{Intra}}, z_2^{\text{Intra}}, Q_{\text{Intra}}) \\ &+ \lambda_{\text{NN}} \cdot \mathcal{L}_{\text{NN}}(z_1^{\text{NN}}, z_2^{\text{NN}}, Q_{\text{NN}}) \end{aligned} \quad (5)$$

Note that class labels are not used and the model is free to learn its own notion of similarity. Over the course of pretraining, the model becomes better at picking semantically similar nearest-neighbor video clips while introducing additional diversity of positive samples that is not possible through sampling intra-video clips, as shown in Fig. 3.

3.3. Pretraining Methodology

3.3.1 Momentum Encoder and Queue

We make several design choices that enable end-to-end learning from unlabeled videos using our method. As contrastive learning requires large batch sizes [7] and computing video embeddings is expensive, we use a FIFO queue that is updated with embeddings from a momentum encoder, similar to [29, 10]. The momentum encoder’s weights θ_k are updated as a moving average of the encoder’s weights θ_q , with momentum coeff. $m \in [0, 1)$, as given by Eq. 6. Thus the momentum encoder receives no gradients.

$$\theta_k \leftarrow m\theta_k + (1 - m)\theta_q \quad (6)$$

We share the same encoder but utilize separate MLP heads when processing intra-video and nearest-neighbor positives. We also maintain two separate queues for each task. Note that the queue contains approximate representations of a large subset of pretraining data in memory and is

dynamically updated “for free” since we only use embeddings that are already computed during the forward pass. Our method scales to large data and is more efficient than methods that utilize clustering such as [4, 41, 5, 51]. Our method also allows for more up-to-date representations than methods that use an offline positive set [45, 6].

3.3.2 Implementation Details

Loss. The temperature $\tau = 0.1$. $\lambda_{Intra} = 1.0$, $\lambda_{NN} = 1.0$.

Encoder. For all experiments, we use a ResNet3D-50 8x8 slow pathway from [19] with He initialization [30], unless otherwise indicated. Outputs are taken after the global average pooling layer to form a 2048-d embedding. Following [10, 20], we use a 3-layer projection MLP during pre-training only. The MLP has hidden dimension 2048 and final embedding dimension of 128 with no batch norm (BN). The MLP is then removed for downstream experiments. As mentioned above, we use two separate MLP heads for producing intra-video and NN embeddings.

Pretraining Hyperparameters. We train for 200 epochs using SGD optimizer (momentum 0.9, weight decay 10^{-4}) with a total batch size of 512. BN statistics are computed per GPU. We linearly warmup the learning rate to 0.4 over the first 35 epochs, then use half-period cosine decay [42].

We use a queue storing 65536 negatives and shuffling-BN to avoid information leakage and overfitting [29]. The momentum encoder weights are updated per Eq. 6 with an annealed momentum coeff. as in [20], initialized to 0.994.

Data and Augmentations We sample two 8-frame clips with a temporal stride of 8 from each video for self-supervised pretraining. We apply random shortest-side resizing to [256, 320] pixels, color jittering (ratio 0.4, p=0.8), grayscale conversion (p=0.2), Gaussian blur (p=0.5), horizontal flip (p=0.2), and random cropping to 224×224 .

4. Experiments

4.1. Baselines

CVRL [52] and ρ -MoCo [20] are two leading contrastive learning works that sample intra-video clips. We primarily compare against ρ -MoCo for $\rho=2$ (two clips per video), pretrained for 200 epochs on unlabeled K400, and call this baseline ρ -MoCo. The original paper does not test ρ -MoCo on all downstream datasets, so we rerun all downstream experiments (even those reported in the paper) for fair comparison. We compare our IIVCL against ρ -MoCo to distill the effect of improved positive key diversity and balanced global-local context on downstream task performance.

4.2. Action Recognition on UCF101, HMDB51, and Kinetics-400

Unless otherwise noted, we train IIVCL on unlabeled K400 [35] (240K videos) for 200 epochs. After self-

supervised pretraining, we transfer the learned weights to target datasets for downstream evaluation. We use two evaluation protocols that are popular in the literature for evaluating the quality of self-supervised representations: **(i) Linear evaluation** freezes the backbone and trains a linear classifier on the target dataset, and **(ii) Finetuning** trains the entire network end-to-end on the target dataset.

We first report top-1 accuracy on three of the most popular action datasets. For UCF101 [54] and HMDB51 [39], we report finetuning top-1 accuracy on split 1. UCF101 contains 9.5K/3.7K train/test videos with 101 action classes, and HMDB51 contains 3.5K/1.5K videos (mostly from movies) with 51 action classes. For K400 [35], we report linear evaluation top-1 accuracy. Kinetics contains 240K/19K train/test videos with 400 action classes. We sample 8×8 clips for all datasets. At test-time, we use standard 10 (temporal) \times 3 (spatial) crop evaluation [19]. We report the avg. of three runs.

4.2.1 Comparison to state-of-the-art.

In Table 1, we compare IIVCL against state-of-the-art self-supervised methods in the literature that use only RGB frames (no optical flow nor audio), as well as our intra-video baseline ρ -MoCo using the protocols introduced at the beginning of Sec. 4.2.

First, we compare IIVCL against the ρ -MoCo baseline to distill the effect of improved positive key diversity and added global context on downstream performance. IIVCL outperforms ρ -MoCo by 1.5% on UCF, 0.5% on HMDB, and by 0.3% on K400. The smaller performance delta on K400 may be due to the fact that linear evaluation is not as reflective of real performance as finetuning the entire network [46]. Consistent improvements over ρ -MoCo highlights the effectiveness of combining intra-video and nearest-neighbor sampling, compared to sampling only intra-video positives.

Next, we compare IIVCL against other methods. IIVCL also outperforms works that trained for more epochs (e.g. VTHCL [68]) or used more frames during pretraining (e.g. SpeedNet [2], VideoMoCo [50]). IIVCL pretrained for 400 epochs surpasses CVRL [52] which pretrained for 2.5x more epochs using 2x more frames.

To fairly compare against other video contrastive learning works, we also present results for a weaker version of our model trained for 200 epochs with a smaller backbone (R18) and smaller input resolution (128x128). Under this setting, our model still convincingly outperforms methods that use larger backbones such as VTHCL [68] and MemDPC [27], and larger input resolution such as VideoMoco [50] and LSF [1].

Method	Date	Backbone	Pretrain Data (duration)	Pretrain Epochs	Pretrain Input Size	UCF	HMDB	K400
Supervised		R3D-50	scratch		8×224^2	68.8	22.7	74.7
DPC [26]	2019	R2D-3D34	K400 (28d)	110	40×224^2	75.7	35.7	-
CBT [56]	2019	S3D	K600+(273d)	130	112^2	79.5	44.6	-
DynamoNet [16]	2019	STCNet	YT8M-1 (58d)	-	32×112^2	88.1	59.5	-
SpeedNet [2]	2020	S3D-G	K400 (28d)	-	16×224^2	81.1	48.8	-
MemDPC [27]	2020	R2D-3D34	K400 (28d)	-	40×224^2	86.1	54.5	-
VideoMoCo [50]	2021	R(2+1)D18	K400 (28d)	200	32×224^2	78.7	49.2	-
TCLR [13]	2021	R(2+1)D18	K400 (28d)	400	16×112^2	84.1	53.6	-
VCLR [38]	2021	R2D-50	K400 (28d)	400	32×224^2	85.6	54.1	64.1
LSFD [1]	2021	R3D-18	K400 (28d)	500	16×224^2	77.2	53.7	-
TECVRL [33]	2021	R3D-18	K400 (28d)	200	16×128^2	87.1	63.6	-
IIVCL		R3D-18	K400 (28d)	200	8×128^2	89.4	60.2	59.2
VTHCL [68]	2020	R3D-50	K400 (28d)	200	8×224^2	82.1	49.2	37.8
CVRL [52]	2020	R3D-50	K400 (28d)	1000	16×224^2	92.2	66.7	66.1
ρ -MoCo [†] [20]	2021	R3D-50	K400 (28d)	200	8×224^2	91.1	65.3	65.4
ρ -MoCo [†] [20]	2021	R3D-50	K400 (28d)	400	8×224^2	92.5	-	67.4
IIVCL		R3D-50	K400 (28d)	200	8×224^2	92.6	65.8	65.7
IIVCL		R3D-50	K400 (28d)	400	8×224^2	93.3	68.1	67.1

Table 1: **Comparison with state-of-the-art self-supervised approaches.** Reported results are top-1 accuracy under finetune protocol (UCF, HMDB) and linear protocol (K400). We do not compare against two-stream methods.

[†] refers to our reimplementation (see Sec. 4.1).

Method	Backbone	Pretrain Data	Top-1 Acc
Supervised [19]	R3D-50	K400	52.8
ρ -MoCo [20]	R3D-50	K400	53.6
IIVCL	R3D-50	K400	53.8

Table 2: **Action recognition on Something-Something.** We finetune on SSv2 using a clip size of 8×8 and report top-1 accuracy.

4.3. Action Recognition on Something-Something v2

To further demonstrate the effectiveness of nearest-neighbor sampling for video contrastive learning, we evaluate IIVCL on Something-Something v2 [23] (SSv2), which is a challenging benchmark focused on understanding granular motions. Unlike UCF101 and HMDB51 which are very similar to K400, SSv2 distinguishes between directionality for the same higher-level action. For example "putting something **into** something" vs. "putting something **next to** something" are different action classes, as well as "moving something up" vs. "pushing something from right to left". We finetune on SSv2 using the same settings as [20].

IIVCL marginally outperforms the ρ -MoCo baseline. As SSv2 is very different in nature from the K400 dataset which we pretrained on, these results further demonstrate that improving positive key diversity and introducing global similarity leads to more generalized video representations that outperform pure intra-video sampling-based methods.

4.4. Action Detection on AVA

Thus far, we have demonstrated that IIVCL can generalize to new domains within the same task of action recognition. To test whether our method can also generalize to novel downstream tasks, we evaluate IIVCL on the new task of action detection, which not only requires accurately classifying the action but also localizing the bounding box of the person performing the action.

We evaluate on the AVA dataset [25] which contains 221K/57K training and validation videos, and report mean Average Precision (mAP) at IOU threshold 0.5. We follow [20] and use our self-supervised trained R3D-50 as the backbone for a Faster R-CNN detector. We then extend the 2D RoI features into 3D along the temporal axis, and apply RoIAlign and temporal global average pooling. The RoI features are then max-pooled and fed to a per-class sigmoid classifier. We also use a similar training schedule as [20], except we train for only 20 epochs with batch size 64, and use an initial learning rate of 0.1 with 10x step-wise learning rate decay at epochs 5, 10, and 15.

IIVCL outperforms the ρ -MoCo baseline on the new task of action detection, on a dataset sourced from cinematic movies rather than Internet videos. IIVCL also outperforms CVRL [52] despite CVRL being trained for 5x more epochs and using 2x more pretraining frames. As AVA is highly different from the unlabeled K400 videos used for pretraining (while UCF101 and HMDB51 are highly similar to K400), this further supports our hypothesis that improved positive key diversity and added global context through nearest-neighbor sampling improves generalization on video tasks.

Method	Pretrain Data	Top-1 Acc
Supervised [19]	K400	21.9
CVRL [52]	K400	16.3
ρ -MoCo [20]	K400	18.6
IIVCL	K400	19.0

Table 3: **Action detection on AVA.** We finetune on AVA using a clip size of 8×8 and report mAP@0.5 IOU.

4.5. Ablations

We perform a series of ablations to validate our design decisions. Unless otherwise indicated, we pretrain on full unlabeled K400 (240K videos), and the same settings as the main experiments, except for the ablated parameters.

4.5.1 MLP Heads

We first ablate the use of separate MLP heads during pretraining. We trained a version of IIVCL that shares the MLP head for both intra-video and NN pairs. In this case, the pretraining loss fails to converge and downstream task results are poor. We hypothesize this is due to the different feature spaces learned for intra-video clips vs. inter-video NNs. Thus, we share the backbone but use separate MLP heads during pretraining. No MLP is used for downstream eval.

4.5.2 Task Generalization of Intra and NN Weights

In Table 6, we summarize the results from above sections in which IIVCL outperformed ρ -MoCo on every dataset per task and per evaluation protocol. We also ablate our choice of λ_{NN} by providing results for $(\lambda_{Intra}=0.0, \lambda_{NN}=1.0)$, and $(\lambda_{Intra}=1.0, \lambda_{NN}=1.0)$. Note that $(\lambda_{Intra}=0.0, \lambda_{NN}=1.0)$ corresponds to a pure NN sampling strategy that uses no intra-video pairs, aka a video-analog of NNCLR [18]. We summarize the average rank per task for each configuration. The best configuration achieves lowest average rank of 1.2.

Pure NN sampling (video analog of NNCLR [18]) is surprisingly competitive with pure intra-video sampling on every task, despite learning zero local semantics during SSL pretraining. However, combining the intra and NN loss $(\lambda_{Intra}=1.0, \lambda_{NN}=1.0)$ does not result in as large of a boost as expected. This may suggest that local and global information are complimentary, but may still provide orthogonal directions that are challenging to learn from.

4.6. Effect of More Epochs and More NNs

Table 8 shows that downstream accuracy increases with the number of temporal samples per video and duration of pretraining. Due to limited compute we do not test more combinations, but expect further room for improvement.

4.7. Few-Shot Learning

Another way to measure the quality of a self-supervised representation is through data efficiency, or how perfor-

Method	UCF Finetune			K400 Linear	
	1%	5%	20%	1%	10%
Supervised (Scratch)				3.2	39.6
ρ -MoCo [20]	41.8	68.0	84.7	34.3	53.3
IIVCL	44.3	68.9	85.0	34.9	54.2
Δ	+2.5	+0.9	+0.3	+0.6	+0.9

Table 4: **Few-shot learning on UCF101 and K400.** Rows indicate different pretrained models on K400. Columns vary the % of UCF training data used for finetuning and % of K400 training data used for linear eval.

Epochs	ρ	UCF	HMDB	K400	SSv2
200	2	92.6	65.8	65.7	53.8
200	4	93.3	67.8	66.6	54.6
400	2	93.3	68.1	67.1	54.2

Table 5: **More pretraining epochs and NNs.** Data is unlabeled K400.

mance varies with respect to the amount of data available for downstream classification [46]. Many works report that self-supervised representations are more data efficient than supervised representations [52, 65, 6, 29].

We first compare against ρ -MoCo on UCF101 using the finetune protocol when training data is limited to 1%, 5%, and 20%, and the evaluation set remains the same. We observe that IIVCL is more data efficient across all three subsets. We then compare against ρ -MoCo on K400 using the linear evaluation protocol when training data is limited to 1% and 10%, and the evaluation set remains the same. We observe similar improvements across both subsets for IIVCL. For both UCF and K400, the delta between IIVCL and ρ -MoCo is largest for the smallest training set of 1% data, indicating that inter-video nearest-neighbors are particularly helpful for generalizing to few-shot settings. We also significantly outperform the supervised baseline in which R3D-50 is initialized from scratch. See Table 4.

4.8. Zero-Shot Video Retrieval

We also evaluate on video retrieval where the extracted features are directly used to find the nearest-neighbors, so there is no further training. Following common practice [28, 67], we use test-set videos to search the k nearest-neighboring video samples from the train set. We evaluate using Recall at k ($R@K$), which means that the retrieval is correct if any of the top k nearest-neighbors are from the same class as the query. See Table 7.

IIVCL outperforms ρ -MoCo for all but one recall threshold on UCF and all recall thresholds on HMDB. This indicates that even without any downstream training, IIVCL is better able to push similar videos of a different downstream dataset closer in the embedding space.

Model		Action Recognition				Action Detection		Avg. Rank
		Finetune			Linear	Finetune		
λ_{Intra}	λ_{NN}	UCF	HMDB	SSv2	K400	AVA		
1.0	0.0	91.1 (#3)	65.3 (#3)	53.6 (#2)	65.4 (#2)	18.6 (#2)		2.4
1.0	1.0	92.6 (#1)	65.8 (#2)	53.8 (#1)	65.7 (#1)	19.0 (#1)		1.2
0.0	1.0	91.2 (#2)	66.2 (#1)	53.2 (#3)	63.7 (#3)	18.4 (#3)		2.4

Table 6: **Do NNs lead to better generalization?** The first row corresponds to the ρ -MoCo baseline and second row corresponds to IIVCL. All models are pretrained on full K400 for 200 epochs. Downstream eval uses clip size of 8×8 . $\lambda_{Intra}=0.0$ means no intra-video positives are used (NNCLR for video). We denote rank in blue parenthesis (where 1st = best) on each task to show the generalization of each model.

Method	Network	Pretrain	UCF				HMDB			
			R@1	R@5	R@10	R@20	R@1	R@5	R@10	R@20
SpeedNet [2]	S3D-G	K400	13.0	28.1	37.5	49.5				
GDT [51]	R(2+1)D	K400	57.4	73.4	80.8	88.1	25.4	51.4	63.9	75.0
VCLR [38]	R2D-50	K400	70.6	80.1	86.3	90.7	35.2	58.4	68.8	79.8
ρ -MoCo [20]	R3D-50	K400	73.2	87.0	91.8	95.5	36.3	61.9	72.0	82.5
IIVCL	R3D-50	K400	74.2	87.6	92.1	95.1	37.6	62.2	72.9	82.5

Table 7: **Zero-shot video retrieval on UCF101 and HMDB.** We do not compare against two-stream methods. This work only uses RGB.

5. Discussion

5.1. Co-Occurrence of Semantic Classes During Pretraining

Although labels are not used during self-supervised pretraining, we analyze the probability that a video in the negative queue belongs to the same class as the query video, to understand why the nearest-neighbor objective is beneficial. Assume the queue samples are uniformly sampled and that each class is balanced. Let the pretraining dataset have K balanced classes, and the queue have Q uniformly sampled samples where Q is smaller than the size of the dataset. Then the probability of the above event is $1 - [(K-1)/K]^Q$, which is well over 0.9 for $K=400$ (number of classes in Kinetics-400), $Q=1024$. Note that this calculation also applies to approaches that sample negatives from the mini-batch; let Q be the mini-batch size. CVRL [52] uses a mini-batch size of 1024 during pretraining. Thus, it is extremely likely that videos belonging to same class as the query are pushed away in the embedding space as negatives in works like [29, 7, 52, 20]. Our work does not address this issue by removing poor choices of negatives from the negative set, but rather leverages those similar videos as additional positive keys for a second loss term via the NN sampling strategy, thus providing additional sources of similarity to learn from that would otherwise be ignored.

Additionally, by dynamically computing the positive key using the learned representation space and sampling videos globally, we allow the model to continually evolve its notion of semantic similarity; the quality of the chosen NNs improves as the model learns as demonstrated by Fig. 3.

With intra-video positive pair sampling, the learned representation is not used to choose the positive pairs — two clips are simply randomly sampled from within a single video.

5.2. Limitations and Future Work

While the focus of our work was on improving the diversity of positive keys and balancing global with local notions of similarity, our method can be improved by reducing false negatives similar to works such as [12]. Our method could also be improved by leveraging audio-video correspondence [45] and exploring more nuanced ways to combine the intra and inter-video positives.

6. Conclusion

We presented IIVCL, which addresses limitations of existing self-supervised contrastive learning works for video [52, 20] that sample only intra-video clips as positives. By leveraging nearest-neighboring samples from a global neighborhood as positives, we expand the positive keyset beyond individual video boundaries, thus improving the diversity of positive keys and blending global with local context. We then demonstrated that our method improves performance over a wide range of video-related tasks, compared to our intra-video contrastive learning baseline. Our method is simple, effective, and directly plugs into existing contrastive frameworks. IIVCL scales to large datasets, unlike methods that require clustering or offline positive sets. We believe that our method has the potential to excel on large unstructured datasets, where self-supervised learning can reach its full potential for video understanding.

References

- [1] Nadine Behrmann, Mohsen Fayyaz, Juergen Gall, and Mehdi Noroozi. Long short view feature decomposition via contrastive video representation learning. In *Proceedings of the IEEE/CVF International Conference on Computer Vision*, pages 9244–9253, 2021.
- [2] Sagie Benaim, Ariel Ephrat, Oran Lang, Inbar Mosseri, William T Freeman, Michael Rubinstein, Michal Irani, and Tali Dekel. Speednet: Learning the speediness in videos. In *Proceedings of the IEEE/CVF Conference on Computer Vision and Pattern Recognition*, pages 9922–9931, 2020.
- [3] Tom B Brown, Benjamin Mann, Nick Ryder, Melanie Subbiah, Jared Kaplan, Prafulla Dhariwal, Arvind Neelakantan, Pranav Shyam, Girish Sastry, Amanda Askell, et al. Language models are few-shot learners. *arXiv preprint arXiv:2005.14165*, 2020.
- [4] Mathilde Caron, Ishan Misra, Julien Mairal, Priya Goyal, Piotr Bojanowski, and Armand Joulin. Unsupervised learning of visual features by contrasting cluster assignments. In *Thirty-fourth Conference on Neural Information Processing Systems (NeurIPS)*, 2020.
- [5] Brian Chen, Andrew Rouditchenko, Kevin Duarte, Hilde Kuehne, Samuel Thomas, Angie Boggust, Rameswar Panda, Brian Kingsbury, Rogerio Feris, David Harwath, et al. Multi-modal clustering networks for self-supervised learning from unlabeled videos. *arXiv preprint arXiv:2104.12671*, 2021.
- [6] Shixing Chen, Xiaohan Nie, David Fan, Dongqing Zhang, Vimal Bhat, and Raffay Hamid. Shot contrastive self-supervised learning for scene boundary detection. In *Proceedings of the IEEE/CVF Conference on Computer Vision and Pattern Recognition*, pages 9796–9805, 2021.
- [7] Ting Chen, Simon Kornblith, Mohammad Norouzi, and Geoffrey Hinton. A simple framework for contrastive learning of visual representations. In *International conference on machine learning*, pages 1597–1607. PMLR, 2020.
- [8] Ting Chen, Simon Kornblith, Kevin Swersky, Mohammad Norouzi, and Geoffrey Hinton. Big self-supervised models are strong semi-supervised learners. *arXiv preprint arXiv:2006.10029*, 2020.
- [9] Weifeng Chen, Shengyi Qian, David Fan, Noriyuki Kojima, Max Hamilton, and Jia Deng. Oasis: A large-scale dataset for single image 3d in the wild. In *Proceedings of the IEEE/CVF Conference on Computer Vision and Pattern Recognition*, pages 679–688, 2020.
- [10] Xinlei Chen, Haoqi Fan, Ross Girshick, and Kaiming He. Improved baselines with momentum contrastive learning, 2020.
- [11] Xinlei Chen and Kaiming He. Exploring simple siamese representation learning. In *Proceedings of the IEEE/CVF Conference on Computer Vision and Pattern Recognition*, pages 15750–15758, 2021.
- [12] Ching-Yao Chuang, Joshua Robinson, Yen-Chen Lin, Antonio Torralba, and Stefanie Jegelka. Debaised contrastive learning. *Advances in neural information processing systems*, 33:8765–8775, 2020.
- [13] Ishan Dave, Rohit Gupta, Mamshad Nayeem Rizve, and Mubarak Shah. Tclr: Temporal contrastive learning for video representation. *arXiv preprint arXiv:2101.07974*, 2021.
- [14] Jia Deng, Wei Dong, Richard Socher, Li-Jia Li, Kai Li, and Li Fei-Fei. Imagenet: A large-scale hierarchical image database. In *Proceedings of the IEEE Conference on Computer Vision and Pattern Recognition*, 2009.
- [15] Jacob Devlin, Ming-Wei Chang, Kenton Lee, and Kristina Toutanova. Bert: Pre-training of deep bidirectional transformers for language understanding. *arXiv preprint arXiv:1810.04805*, 2018.
- [16] Ali Diba, Vivek Sharma, Luc Van Gool, and Rainer Stiefelhagen. Dynamonet: Dynamic action and motion network. In *Proceedings of the IEEE/CVF International Conference on Computer Vision*, pages 6192–6201, 2019.
- [17] Carl Doersch, Abhinav Gupta, and Alexei A Efros. Unsupervised visual representation learning by context prediction. In *Proceedings of the IEEE international conference on computer vision*, pages 1422–1430, 2015.
- [18] Debidatta Dwivedi, Yusuf Aytar, Jonathan Tompson, Pierre Sermanet, and Andrew Zisserman. With a little help from my friends: Nearest-neighbor contrastive learning of visual representations. In *Proceedings of the IEEE/CVF International Conference on Computer Vision (ICCV)*, pages 9588–9597, October 2021.
- [19] Christoph Feichtenhofer, Haoqi Fan, Jitendra Malik, and Kaiming He. Slowfast networks for video recognition. In *Proceedings of the IEEE/CVF international conference on computer vision*, pages 6202–6211, 2019.
- [20] Christoph Feichtenhofer, Haoqi Fan, Bo Xiong, Ross Girshick, and Kaiming He. A large-scale study on unsupervised spatiotemporal representation learning. In *Proceedings of the IEEE/CVF Conference on Computer Vision and Pattern Recognition*, pages 3299–3309, 2021.
- [21] Basura Fernando, Hakan Bilen, Efstratios Gavves, and Stephen Gould. Self-supervised video representation learning with odd-one-out networks. In *Proceedings of the IEEE conference on computer vision and pattern recognition*, pages 3636–3645, 2017.
- [22] Spyros Gidaris, Praveer Singh, and Nikos Komodakis. Unsupervised representation learning by predicting image rotations. *arXiv preprint arXiv:1803.07728*, 2018.
- [23] Raghav Goyal, Samira Ebrahimi Kahou, Vincent Michalski, Joanna Materzynska, Susanne Westphal, Heuna Kim, Valentin Haenel, Ingo Fruend, Peter Yianilos, Moritz Mueller-Freitag, et al. The” something something” video database for learning and evaluating visual common sense. In *Proceedings of the IEEE international conference on computer vision*, pages 5842–5850, 2017.
- [24] Jean-Bastien Grill, Florian Strub, Florent Altché, Corentin Tallec, Pierre Richemond, Elena Buchatskaya, Carl Doersch, Bernardo Pires, Zhaohan Guo, Mohammad Azar, et al. Bootstrap your own latent: A new approach to self-supervised learning. In *Neural Information Processing Systems*, 2020.
- [25] Chunhui Gu, Chen Sun, David A Ross, Carl Vondrick, Caroline Pantofaru, Yeqing Li, Sudheendra Vijayanarasimhan, George Toderici, Susanna Ricco, Rahul Sukthankar, et al.

- Ava: A video dataset of spatio-temporally localized atomic visual actions. In *Proceedings of the IEEE Conference on Computer Vision and Pattern Recognition*, pages 6047–6056, 2018.
- [26] Tengda Han, Weidi Xie, and Andrew Zisserman. Video representation learning by dense predictive coding. In *Proceedings of the IEEE/CVF International Conference on Computer Vision Workshops*, pages 0–0, 2019.
- [27] Tengda Han, Weidi Xie, and Andrew Zisserman. Memory-augmented dense predictive coding for video representation learning. In *Computer Vision—ECCV 2020: 16th European Conference, Glasgow, UK, August 23–28, 2020, Proceedings, Part III 16*, pages 312–329. Springer, 2020.
- [28] Tengda Han, Weidi Xie, and Andrew Zisserman. Self-supervised co-training for video representation learning. *Advances in Neural Information Processing Systems*, 33:5679–5690, 2020.
- [29] Kaiming He, Haoqi Fan, Yuxin Wu, Saining Xie, and Ross Girshick. Momentum contrast for unsupervised visual representation learning. In *Proceedings of the IEEE/CVF Conference on Computer Vision and Pattern Recognition*, pages 9729–9738, 2020.
- [30] Kaiming He, Xiangyu Zhang, Shaoqing Ren, and Jian Sun. Delving deep into rectifiers: Surpassing human-level performance on imagenet classification. In *Proceedings of the IEEE international conference on computer vision*, pages 1026–1034, 2015.
- [31] Qingqiu Huang, Yu Xiong, Anyi Rao, Jiase Wang, and Dahua Lin. Movienet: A holistic dataset for movie understanding. In *Computer Vision—ECCV 2020: 16th European Conference, Glasgow, UK, August 23–28, 2020, Proceedings, Part IV 16*, pages 709–727. Springer, 2020.
- [32] Allan Jabri, Andrew Owens, and Alexei Efros. Space-time correspondence as a contrastive random walk. *Advances in neural information processing systems*, 33, 2020.
- [33] Simon Jenni and Hailin Jin. Time-equivariant contrastive video representation learning. In *Proceedings of the IEEE/CVF International Conference on Computer Vision*, pages 9970–9980, 2021.
- [34] Longlong Jing, Xiaodong Yang, Jingen Liu, and Yingli Tian. Self-supervised spatiotemporal feature learning via video rotation prediction. *arXiv preprint arXiv:1811.11387*, 2018.
- [35] Will Kay, Joao Carreira, Karen Simonyan, Brian Zhang, Chloe Hillier, Sudheendra Vijayanarasimhan, Fabio Viola, Tim Green, Trevor Back, Paul Natsev, et al. The kinetics human action video dataset. *arXiv preprint arXiv:1705.06950*, 2017.
- [36] Dahun Kim, Donghyeon Cho, and In So Kweon. Self-supervised video representation learning with space-time cubic puzzles. In *Proceedings of the AAAI Conference on Artificial Intelligence*, volume 33, pages 8545–8552, 2019.
- [37] Alexander Kolesnikov, Xiaohua Zhai, and Lucas Beyer. Revisiting self-supervised visual representation learning. In *Proceedings of the IEEE/CVF conference on computer vision and pattern recognition*, pages 1920–1929, 2019.
- [38] Haofei Kuang, Yi Zhu, Zhi Zhang, Xinyu Li, Joseph Tighe, Soren Schwertfeger, Cyrill Stachniss, and Mu Li. Video contrastive learning with global context. In *Proceedings of the IEEE/CVF International Conference on Computer Vision*, pages 3195–3204, 2021.
- [39] Hildegard Kuehne, Hueihan Jhuang, Estibaliz Garrote, Tomaso Poggio, and Thomas Serre. Hmdb: a large video database for human motion recognition. In *2011 International conference on computer vision*, pages 2556–2563. IEEE, 2011.
- [40] Hsin-Ying Lee, Jia-Bin Huang, Maneesh Singh, and Ming-Hsuan Yang. Unsupervised representation learning by sorting sequences. In *Proceedings of the IEEE International Conference on Computer Vision*, pages 667–676, 2017.
- [41] Junnan Li, Pan Zhou, Caiming Xiong, and Steven CH Hoi. Prototypical contrastive learning of unsupervised representations. *arXiv preprint arXiv:2005.04966*, 2020.
- [42] Ilya Loshchilov and Frank Hutter. Sgdr: Stochastic gradient descent with warm restarts. *arXiv preprint arXiv:1608.03983*, 2016.
- [43] Zelun Luo, Boya Peng, De-An Huang, Alexandre Alahi, and Li Fei-Fei. Unsupervised learning of long-term motion dynamics for videos. In *Proceedings of the IEEE conference on computer vision and pattern recognition*, pages 2203–2212, 2017.
- [44] Ishan Misra, C Lawrence Zitnick, and Martial Hebert. Shuffle and learn: unsupervised learning using temporal order verification. In *European Conference on Computer Vision*, pages 527–544. Springer, 2016.
- [45] Pedro Morgado, Nuno Vasconcelos, and Ishan Misra. Audio-visual instance discrimination with cross-modal agreement. In *Proceedings of the IEEE/CVF Conference on Computer Vision and Pattern Recognition*, pages 12475–12486, 2021.
- [46] Alejandro Newell and Jia Deng. How useful is self-supervised pretraining for visual tasks? In *Proceedings of the IEEE/CVF Conference on Computer Vision and Pattern Recognition*, pages 7345–7354, 2020.
- [47] Mehdi Noroozi and Paolo Favaro. Unsupervised learning of visual representations by solving jigsaw puzzles. In *European conference on computer vision*, pages 69–84. Springer, 2016.
- [48] Mehdi Noroozi, Hamed Pirsiavash, and Paolo Favaro. Representation learning by learning to count. In *Proceedings of the IEEE International Conference on Computer Vision*, pages 5898–5906, 2017.
- [49] Aaron van den Oord, Yazhe Li, and Oriol Vinyals. Representation learning with contrastive predictive coding. *arXiv preprint arXiv:1807.03748*, 2018.
- [50] Tian Pan, Yibing Song, Tianyu Yang, Wenhao Jiang, and Wei Liu. Videomoco: Contrastive video representation learning with temporally adversarial examples. In *Proceedings of the IEEE/CVF Conference on Computer Vision and Pattern Recognition*, pages 11205–11214, 2021.
- [51] Mandela Patrick, Yuki M Asano, Polina Kuznetsova, Ruth Fong, Joao F Henriques, Geoffrey Zweig, and Andrea Vedaldi. Multi-modal self-supervision from generalized data transformations. *arXiv preprint arXiv:2003.04298*, 2020.
- [52] Rui Qian, Tianjian Meng, Boqing Gong, Ming-Hsuan Yang, Huisheng Wang, Serge Belongie, and Yin Cui. Spatiotemporal contrastive video representation learning. In *Proceedings*

- of the *IEEE/CVF Conference on Computer Vision and Pattern Recognition*, pages 6964–6974, 2021.
- [53] Adrià Recasens, Pauline Luc, Jean-Baptiste Alayrac, Luyu Wang, Ross Hemsley, Florian Strub, Corentin Tallec, Mateusz Malinowski, Viorica Patraucean, Florent Altché, Michal Valko, Jean-Bastien Grill, Aäron van den Oord, and Andrew Zisserman. Broaden your views for self-supervised video learning, 2021.
- [54] Khurram Soomro, Amir Roshan Zamir, and Mubarak Shah. Ucf101: A dataset of 101 human actions classes from videos in the wild. *arXiv preprint arXiv:1212.0402*, 2012.
- [55] Nitish Srivastava, Elman Mansimov, and Ruslan Salakhudinov. Unsupervised learning of video representations using lstms. In *International conference on machine learning*, pages 843–852. PMLR, 2015.
- [56] Chen Sun, Fabien Baradel, Kevin Murphy, and Cordelia Schmid. Contrastive bidirectional transformer for temporal representation learning, 2019a. URL <http://arxiv.org/abs/1906>.
- [57] Chen Sun, Abhinav Shrivastava, Saurabh Singh, and Abhinav Gupta. Revisiting unreasonable effectiveness of data in deep learning era. In *Proceedings of the IEEE international conference on computer vision*, pages 843–852, 2017.
- [58] Yonglong Tian, Dilip Krishnan, and Phillip Isola. Contrastive multiview coding. In *Computer Vision—ECCV 2020: 16th European Conference, Glasgow, UK, August 23–28, 2020, Proceedings, Part XI 16*, pages 776–794. Springer, 2020.
- [59] Carl Vondrick, Hamed Pirsiavash, and Antonio Torralba. Anticipating visual representations from unlabeled video. In *Proceedings of the IEEE conference on computer vision and pattern recognition*, pages 98–106, 2016.
- [60] Jiangliu Wang, Jianbo Jiao, Linchao Bao, Shengfeng He, Yunhui Liu, and Wei Liu. Self-supervised spatio-temporal representation learning for videos by predicting motion and appearance statistics. In *Proceedings of the IEEE/CVF Conference on Computer Vision and Pattern Recognition*, pages 4006–4015, 2019.
- [61] Jiangliu Wang, Jianbo Jiao, and Yun-Hui Liu. Self-supervised video representation learning by pace prediction. In *European conference on computer vision*, pages 504–521. Springer, 2020.
- [62] Xiaolong Wang and Abhinav Gupta. Unsupervised learning of visual representations using videos. In *Proceedings of the IEEE international conference on computer vision*, pages 2794–2802, 2015.
- [63] Xiaolong Wang, Allan Jabri, and Alexei A Efros. Learning correspondence from the cycle-consistency of time. In *Proceedings of the IEEE/CVF Conference on Computer Vision and Pattern Recognition*, pages 2566–2576, 2019.
- [64] Donglai Wei, Joseph J Lim, Andrew Zisserman, and William T Freeman. Learning and using the arrow of time. In *Proceedings of the IEEE Conference on Computer Vision and Pattern Recognition*, pages 8052–8060, 2018.
- [65] Fanyi Xiao, Joseph Tighe, and Davide Modolo. Modist: Motion distillation for self-supervised video representation learning, 2021.
- [66] Tete Xiao, Xiaolong Wang, Alexei A Efros, and Trevor Darrell. What should not be contrastive in contrastive learning. *arXiv preprint arXiv:2008.05659*, 2020.
- [67] Dejing Xu, Jun Xiao, Zhou Zhao, Jian Shao, Di Xie, and Yueting Zhuang. Self-supervised spatiotemporal learning via video clip order prediction. In *Proceedings of the IEEE/CVF Conference on Computer Vision and Pattern Recognition*, pages 10334–10343, 2019.
- [68] Ceyuan Yang, Yinghao Xu, Bo Dai, and Bolei Zhou. Video representation learning with visual tempo consistency. *arXiv preprint arXiv:2006.15489*, 2020.
- [69] Richard Zhang, Phillip Isola, and Alexei A Efros. Colorful image colorization. In *European conference on computer vision*, pages 649–666. Springer, 2016.
- [70] Yi Zhu, Xinyu Li, Chunhui Liu, Mohammadreza Zolfaghari, Yuanjun Xiong, Chongruo Wu, Zhi Zhang, Joseph Tighe, R Manmatha, and Mu Li. A comprehensive study of deep video action recognition. *arXiv preprint arXiv:2012.06567*, 2020.
- [71] Chengxu Zhuang, Alex Lin Zhai, and Daniel Yamins. Local aggregation for unsupervised learning of visual embeddings. In *Proceedings of the IEEE/CVF International Conference on Computer Vision*, pages 6002–6012, 2019.

A. Other Experiments

A.1. Effect of Weight Initialization

One potential bottleneck to performance is whether random initialization makes it difficult to pick quality NNs during self-supervised pretraining. To explore this, we tried initializing the model with weights with ρ -*MoCo* pretrained for 200 epochs ($\lambda_{Intra} = 1.0$, $\lambda_{NN} = 0.0$). We then train for 200 more epochs with ($\lambda_{Intra} = 1.0$, $\lambda_{NN} = 1.0$). Note that the effective number of epochs is then 400. Comparing random init at 400 epochs to the pretrained weight init at 200 epochs, there is not a significant improvement. This indicates that figuring out better ways of blending inter-video NNs and intra-video pairs is a topic for future research.

Weight Init	Pretrain Epochs	UCF	HMDB	K400	SSv2
Random	200	92.6	65.8	65.7	53.8
Random	400	93.3	68.1	67.1	52.2
ρ - <i>MoCo</i>	200 (+200)	92.9	67.7	66.8	54.3

Table 8: IIVCL from random initialization vs. ρ -*MoCo* weight initialization. Both are trained for 200 epochs with $\rho=200$ on unlabeled K400.

B. Additional Implementation Details

B.1. Downstream Evaluation Details

We mostly follow [20] for downstream eval.

B.1.1 UCF and HMDB Action Recognition

We randomly sample a 8×8 clip and finetune with the same augmentation as during pretraining, but without Gaussian blur. We train for 200 epochs using a batch size of 64 and a base learning rate of 0.005 (8 GPUs) with half period cosine decay. Weight decay is $1e-4$ and dropout is 0.5. At test-time, we use standard 10x3 crop evaluation [19].

B.1.2 Kinetics-400 Action Recognition

We train a linear classifier on top of the frozen backbone and do not ℓ_2 normalize the embeddings. We randomly sample a 8×8 clip, randomly resize the shortest side to [256, 320], apply random cropping to 224×224 , and random horizontal flip. We train for 60 epochs using a batch size of 512 and a base learning rate of 0.5 (8 GPUs) with half period cosine decay. Weight decay is 0.0 and dropout is 0.0. At test-time, we use standard 10x3 crop evaluation [19].

B.1.3 Something-Something v2 Action Recognition

We randomly sample a 8×8 clip following the same segment-based frame sampling procedure as [20]. We apply

the same augmentations as for K400, but remove flipping because directionality constitutes different action classes in SSv2. We train for 22 epochs using a batch size of 64 and base learning rate of 0.12 (8 GPUs) with 10x step-wise learning rate decay at epochs 14 and 18. Weight decay is 10^{-6} and dropout is 0.5. At test-time, we use a single centered 8×8 clip for evaluation.

B.1.4 AVA Action Detection

We randomly sample a 8×8 clip and finetune with the same augmentations as for K400. We train for 20 epochs with linear warm-up for first 5 epochs, using a batch size of 64 and base learning rate of 0.1 with step-wise 10x decay at epochs 5, 10, and 15. Weight decay is 10^{-7} and dropout is 0.5.

We follow the same region proposal extraction procedure as [20]. We use an off-the-shelf person detector that is not jointly trained with the action detection models. Specifically we use the predictions provided by the Faster R-CNN with ResNeXt-101-FPN backbone that is provided by the SlowFast [19] codebase. At test-time, we use a single centered 8×8 clip for evaluation.

B.2. Encoder Architecture

Our default encoder is a R3D-50 Slow model [19], with a temporal dimension of size $T=8$ and sample rate $\tau=8$. Architecture diagram is given in Table 9.

C. Additional Qualitative Results

We provide additional qualitative examples to help visualize what the model is learning.

C.1. Nearest-Neighbor Evolution During Pretraining

In Figure 4, we show how the nearest-neighbors vary over the course of pre-training, starting from random initialization. We observe that as training progresses, the nearest-neighbors become more semantically similar, which complements Figure 3b) of the main paper.

C.2. Downstream Zero-Shot Retrieval

As mentioned in §4.8 of the main paper, extracted features from the test set are directly used to retrieve nearest-neighboring training set samples. No further training is done. While our retrieved results may sometimes belong to a different class as the query, they are still semantically similar to the query.

D. Self-Supervised Pre-Training Visualizations

To provide a visualization of the semantic feature clusters during the course of unsupervised pretraining on K400,

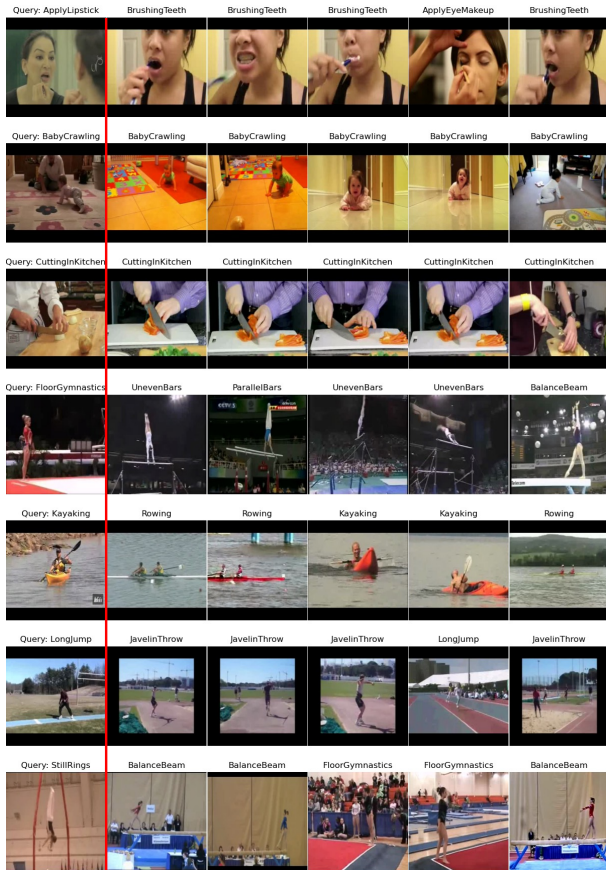
stage	kernels	output sizes $T \times S^2$
raw clip	-	$T\tau \times 224^2$
data layer	stride τ , 1^2	$T \times 224^2$
conv ₁	<u>1×7^2</u> , 64 stride 1, 2^2	$T \times 112^2$
pool ₁	<u>1×3^2</u> max stride 1, 2^2	$T \times 56^2$
res ₂	($\times 3$) <u>1×1^2</u> , 64 <u>1×3^2</u> , 64 <u>1×1^2</u> , 256	$T \times 56^2$
res ₃	($\times 4$) <u>1×1^2</u> , 128 <u>1×3^2</u> , 128 <u>1×1^2</u> , 512	$T \times 28^2$
res ₄	($\times 6$) <u>3×1^2</u> , 256 <u>1×3^2</u> , 256 <u>1×1^2</u> , 1024	$T \times 14^2$
res ₅	($\times 3$) <u>3×1^2</u> , 512 <u>1×3^2</u> , 512 <u>1×1^2</u> , 2048	$T \times 7^2$
pool ₅	global average pool	1×1^2

Table 9: We use the R3D-50 Slow pathway [19] as our 3D encoder for self-supervised learning. The dimensions of kernels are given as $\{T \times S^2, C\}$ for temporal, spatial, and channel sizes. Strides are given as {temporal stride, spatial stride²}. Non-degenerate temporal filters are underlined. Temporal pooling is only performed at the last layer to collapse the space and time dimensions. By default, we sample clips at $T \times \tau = 8 \times 8$.

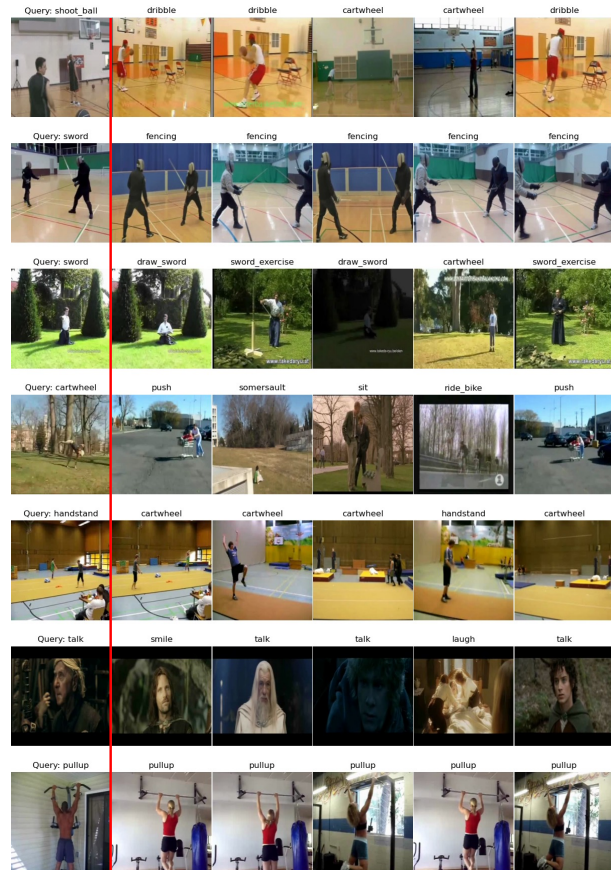
we plotted t-SNE feature visualization on UCF101. The model is not finetuned on UCF. With more pre-training, the features organize into semantically related clusters. For example, “ApplyEyeMakeup” and “ApplyLipstick” cluster together because they are acts of applying cosmetics.



Figure 4: Evolution of inter-video nearest-neighbor positives during pretraining, starting from random initialization. Videos are sampled across the dataset using similarity measured by the learned feature space, which improves during pretraining. Top row is the query video while other rows indicate different epochs of pretraining.



(a) UCF101 retrieval results.



(b) HMDB51 retrieval results.

Figure 5: Video retrieval results for IIVCL on a) UCF101 and b) HMDB51. The left-most column shows the query video while the remaining columns show the top-5 nearest neighbors.

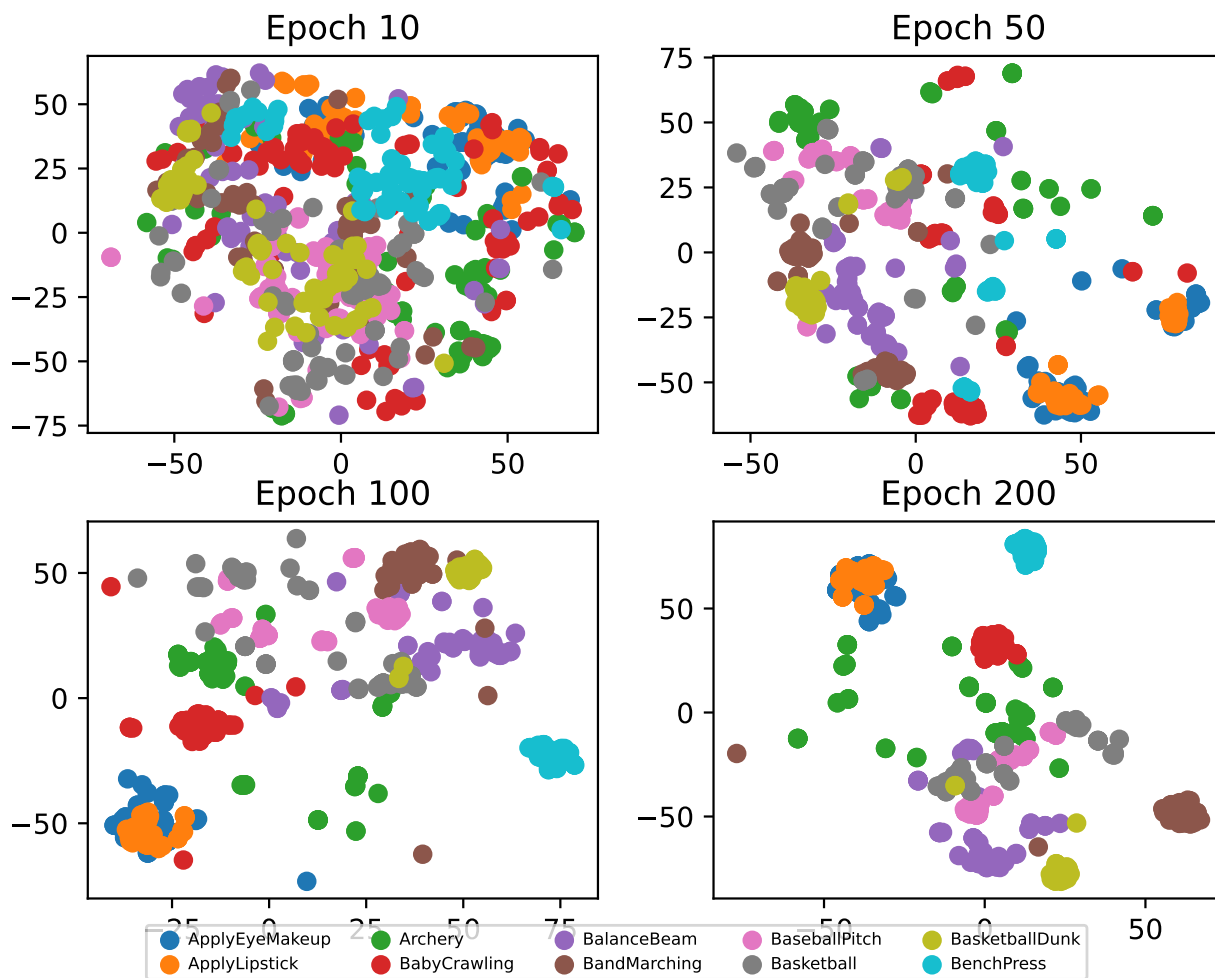


Figure 6: t-SNE feature visualization over epochs of pre-training.

E. Pseudocode

In Algorithm 1, we present the pretraining pseudocode for IIVCL. Note that our approach does not require the usage of momentum encoders. Algorithm 2 shows the pretraining pseudocode **without** momentum encoders.

Algorithm 1: Pseudocode for IIVCL pretraining with momentum encoder.

```
# f-q: online encoder
# g-q-intra, g-q-nn: online projection MLP for intra loss and NN loss
# f-k: momentum encoder
# g-k-intra, g-k-nn: momentum projection MLP for intra loss and NN loss
# m: momentum update coeff.
# intra-queue, nn-queue: queue for intra loss (KxC) and NN loss (KxC)
# intra_lambda, nn_lambda: intra loss and NN loss weights

# load minibatch with N samples. Two clips x1, x2 are sampled from each video.
for (x1, x2) in loader:
    x1, x2 = aug(x1), aug(x2) # random augmentation
    q1, q2 = f.q(x1), f.q(x2) # forward pass to online encoder (NxC)
    # Apply online projection MLPs to view 1
    q1_intra, q1_nn = g.q.intra(q1), g.q.nn(q1)
    # Apply online projection MLPs to view 2
    q2_intra, q2_nn = g.q.intra(q2), g.q.nn(q2)
    k1, k2 = f.k(x1), f.k(x2) # forward pass to momentum encoder (NxC)
    # Apply momentum projection MLPs to view 1
    k1_intra, k1_nn = g.k.intra(k1), g.k.nn(k1)
    # Apply momentum projection MLPs to view 2
    k2_intra, k2_nn = g.k.intra(k2), g.k.nn(k2)
    # No gradients to keys
    k1_intra, k1_nn, k2_intra, k2_nn = detach(k1_intra, k1_nn, k2_intra, k2_nn)

    # Symmetric loss
    total_loss = L(q1_intra, q1_nn, k2_intra, k2_nn) +
                L(q2_intra, q2_nn, k1_intra, k1_nn)
    total_loss.backward() # backprop
    update(f.q.params), update(g.q.intra.params), update(g.q.nn.params) # SGD update
    # update momentum encoder
    f.k.params = m * f.k.params + (1-m) * f.q.params
    g.k.intra.params = m * g.k.intra.params + (1-m) * g.q.intra.params
    g.k.nn.params = m * g.k.nn.params + (1-m) * g.q.nn.params
    # update queues
    update.queue(intra.queue, k1_intra)
    update.queue(nn.queue, k1_nn)

def L(q_intra, q_nn, k_intra, k_nn, intra_lambda=1.0, nn_lambda=0.2):
    nn_idx, nn_loss = L_NN(q_nn, k_nn, nn.queue)
    intra_loss = L_Intra(q_intra, k_intra, nn_idx, intra.queue)
    return intra_lambda * intra_loss + nn_lambda * nn_loss

def L_NN(q, k, nn.queue):
    q, k = normalize(q, dim=1), normalize(k, dim=1) # L2 normalize the embeddings
    # find the location of the nearest-neighbor of k1_nn and k2_nn in nn-queue
    nn_idx = NN(k, nn.queue) # N
    nn_logits = mm(q.view(N,C), nn.queue.view(C,K)) # nn_logits: NxK
    nn_loss = cross_entropy(nn_logits, nn_idx)
    return nn_idx, nn_loss

def L_Intra(q, k, nn_idx, intra.queue):
    q, k = normalize(q, dim=1), normalize(k, dim=1) # L2 normalize the embeddings
    # maskout nearest-neighbor positives from intra-queue
    intra_mask = ones(intra.queue.shape[0]) # mask: KxI
    intra_mask[nn_idx] = False
    masked_intra_queue = intra.queue[intra_mask]
    # intra positive logits: NxI
    intra_logits_positive = bmm(q.view(N,1,C), k.view(N,C,1))
    # intra negative logits: NxK
    intra_logits_negative = mm(q.view(N,C), masked_intra_queue.view(C,K))
    # intra logits: N x(I+K)
    intra_logits = cat([intra_logits_positive, intra_logits_negative], dim=1)
    intra_label = zeros(N)
    intra_loss = cross_entropy(intra_logits, intra_label)
    return intra_loss

# find the location of nearest-neighbor embedding in the queue
def NN(z,Q):
    z = normalize(z, dim=1), Q = normalize(Q, dim=1) # L2 normalize
    # z: input embedding minibatch, NxC
    nn_idx = (z@Q.T).argmax(dim=1) # NN location: NxI
    return nn_idx
```

Algorithm 2: Pseudocode for IIVCL pretraining without momentum encoder.

```
# f: encoder
# g_intra, g_nn: online projection MLP for intra loss and NN loss
# queue: queue for NN loss (KxC)
# intra_lambda, nn_lambda: intra loss and NN loss weights

# load minibatch with N samples. Two clips x1, x2 are sampled from each video.
for (x1, x2) in loader:
    x1, x2 = aug(x1), aug(x2) # random augmentation
    q1, q2 = f(x1), f(x2) # forward pass to online encoder (Nx C)
    q1_intra, q1_nn = g_intra(q1), g_nn(q1) # Apply online projection MLPs to view 1
    q2_intra, q2_nn = g_intra(q2), g_nn(q2) # Apply online projection MLPs to view 2

    # Symmetric loss
    total_loss = intra_lambda * L(q1_intra, q2_intra) + \
        nn_lambda * (L(q1_nn, NN(q2_nn.queue)) + L(q2_nn, NN(q1_nn.queue)))

    total_loss.backward() # backprop
    update(f.params), update(g_intra.params), update(g_nn.params) # SGD update

# update queues
update_queue(nn.queue, q1_nn)

def L(q, k, temperature=0.1):
    q, k = normalize(q, dim=1), normalize(k, dim=1) # L2 normalize the embeddings
    logits = q@k.T # nn_logits: NxN
    logits /= temperature # apply contrastive loss temperature
    logits_idx = range(0,N)
    contrastive_loss = cross_entropy(logits, logits_idx)
    return contrastive_loss

# return nearest-neighbor embedding in the queue
def NN(z,Q):
    z = normalize(z, dim=1), Q = normalize(Q, dim=1) # L2 normalize
    # z: input embedding minibatch, Nx C
    nn_idx = (z@Q.T).argmax(dim=1) # NN location: Nx1
    return Q[nn_idx]
```
